Supplementary Information: Cross-sectional entomological data reveals an increased risk of arboviral transmission in a year of record-breaking heat in Southern Europe

Chiara Virgillito[1], Eleonora Longo[1,2], Carlo Maria De Marco[1], Chiara Gentile[1], Martina Micocci[1], Christos Topalidis[1], Luana Violante[3], Federico Filipponi[4], Piero Poletti[5], Stefano Merler[5], Alessandra della Torre[1], Beniamino Caputo[1*], Mattia Manica[5*]

Affiliation

[1] -Department of Public Health and Infectious Diseases, Sapienza University of Rome, Rome, Italy

[2]- Center Agriculture Food Environment, University of Trento, San Michele all'Adige (TN), Italy

[3] - National PhD Programme in One Health approaches to infectious diseases and life science research, University of Pavia, Pavia, Italy.

[4] - National Research Council – Institute for Environmental Geology and Geoengineering (CNR-IGAG), Montelibretti (Rome), Italy

[5] -Center for Health Emergencies, Fondazione Bruno Kessler, Trento, Italy

*=corresponding authors

Email: mmanica@fbk.eu, beniamino.caputo@uniroma1.it

keywords: outbreak, arbovirus, Aedes, chikungunya, dengue

Contents

Supplementary Notes 1. Description of sampling sites

The sampling area (~1,285 km2) represents the densely populated and historically significant central part of Rome. The urban heat island effect is notable, leading to higher temperatures compared to surrounding rural areas [1,2]. The metropolitan city is delimited by the Grande Raccordo Anulare (GRA), the 68-km long ring-shaped highway encircling the city' most urbanised area. Land use within the GRA is predominantly urban, with residential, commercial, historical and tourist areas interspersed with green spaces such as parks and gardens.

The sampling sites in common between 2012 and 2023 are:

- Muratella is a commercial site inside the Metropolitan area of Rome, although inside the GRA, is characterized by a high density of office buildings and enterprises, making it a significant business hub where people are transitional and move during the day.
- Villa Bonelli is a residential neighbourhood located in the southwestern part of Rome city centre, and it is characterized by green spaces and apartments.
- Trastevere is a historical area located on the west bank of the Tevere River. It represents a tourist site and a cultural hotspot due to the presence of numerous bars, restaurants and artisan shops.
- Arco di Travertino is a densely cemented residential area.
- Vittorio Emanuele, in the proximity of Termini train station, is a commercial and multiethnic residential hub with a relatively big green central area. It represents a tourist spot and a pivotal area for people's passage.
- Cornelia is a green residential area.
- Cipro is a residential and commercial area located near the Vatican City. Due to the vicinity of the Vatican, it is a hotspot for tourists and pilgrims.
- Flaminio is a historical area known for cultural landmarks such as the Auditorium "Parco Della Musica" and the MAXXI Museum of 21st Century Arts. Many private sporting and child educational centres are present. The area is a highly touristic hotspot due to the vicinity to Piazza del Popolo and the entrance to one of the biggest green historical areas of Rome, Villa Borghese.
- Nomentana is a highly populated residential areas in the periphery of Rome City Centre.
- Nuovo Salario is a highly populated residential areas in the periphery of Rome City Centre.

The sampling sites added in 2023 are:

- Roma Aurelia is a peripheric residential neighbourhood encompassed by wide green spaces.
- Subaugusta is a highly populated residential area well connected to the Metro station, representing a high travelling zone.
- Sapienza is the biggest University of Rome. It is located near the two train stations of Termini and Tiburtina, representing a highly populated area visited by students and commuters. Also, Sapienza is near one of the biggest cemeteries in Rome (Verano), which represents a big and humid green area.
- Roma S. Pietro is also located inside GRA, but its main characteristic is its proximity to St. Peter's Basilica and other major religious and historical touristic sites.

Supplementary Methods 1. Mosquito Population model

We calibrated a mosquito population model already applied for the estimation of the mosquito population in Rome [3] and other settings [4]. The model aims to mimic the dynamics of each life-stage of the *Aedes albopictus* population within each site and a single mosquito season. The model equations are the following:

$$\begin{cases} \dot{E} = n_E d_V V - (d_E + m_E)E \\ \dot{L} = d_E E - (m_L \left(1 + \frac{L}{a_{S,y}}\right) + d_L)L \\ \dot{P} = d_L L - (d_P + m_P)P \\ \dot{V} = \frac{1}{2} d_P P - (\sigma * m_V + b)V \end{cases} \quad (1)$$

where:

- E, L, P and V represent the number of eggs, larvae, pupae and female adults respectively.
- n_E is the average number of deposed eggs per female adult per oviposition
- d_V is the temperature-dependent rate of egg deposition for female adults.
- d_E, d_L and d_P are the temperature-dependent rates of progression to the following developmental stage; the coefficient ½ in the equation of female adults (V) accounts for the sex ratio in the development of pupae into adults.
- m_E, m_P, m_L and m_V are temperature-dependent mortality rates for each stage.
- $a_{S,y}$ is the site (s)-year (y)-specific larval carrying capacity.
- b is the Sticky trap[5] capture rate. We estimated the capture rate of Sticky traps from mark-release-recapture experiment [6] rescaled to an area of 300m radius.
- σ is the correction factor for adult mortality.

We reported all parameter values and functional forms of the temperature-dependent rates in Supplementary Table 1. The functional forms expressing the temperature dependence of the 8 rates were estimated in a previously published study[7] using experimental data [8].

Supplementary Methods 2. Calibration procedure

The model population is initialised on 1st March for each year with all state variables set to zero except for fixed initial mosquito eggs (N_E= 1,000), subject to sensitivity analysis; each day, the value of temperature-dependent rates is recomputed based on the average daily temperature registered in each study site. Free model parameters were the carrying capacities ($a_{S,y}$) for each site *s* and year *y*. The carrying capacity represents a measure of the habitat suitability. The carrying capacities for the 2012 sites as well as the correction factor were already estimated in Manica et al., (2017)[3]. Here, we assumed that the correction factor accounting for an increase in mortality rate under field conditions concerning the mortality rate estimated in laboratory settings could be considered constant across sites and years. We estimated 2023 carrying capacities by using a Monte Carlo Markov Chain (hereafter MCMC) procedure based on a Poisson likelihood to calibrate the model against the observed number of captured adult female *Aedes albopictus*, as described fully in Guzzetta et al., (2016) [4]. The convergence of MCMC (30.000 iterations) was assessed by considering several starting points and by visual inspection, after a burn-in period of 5000 iterations. Posterior means and 95% CI of estimates of the site- and year-specific larval carrying capacity, as estimated by the MCMC procedures, are reported in Supplementary Table 2.

Supplementary Methods 3. Model sensitivity to the initial number of eggs

To verify that the model predictions are robust concerning the corresponding assumed value of the initial number of eggs at the beginning of the mosquito season, N_E, set to 1,000 in the main analysis a sensitivity analysis was carried out. To this aim, we run the model with values of equal to 100 and 10.000. Similar to what was found by Guzzetta et al., (2016) [4] the estimated *Ae. albopictus* females per hectare were similar when considering alternative assumptions on model initial conditions in terms of the number of eggs in March. When using N_E= 100, a slightly lower peak mosquito density was found compared to the baseline (N_E=1,000). For N_E= 10,000, the mosquito density overlapped the main mosquito abundance in each site (Supplementary Figure 5-6).

Supplementary Method 4. Comparison of observed and modelled captures

Supplementary Figure 1-2 compares the observed (black point) and modelled (boxplot; median and Interquartile) numbers of adult females *Ae. albopictus*/site captured weekly in 2012 and 2023. The Figure show that the seasonal pattern is correctly reproduced by the model. Sites with a low R^2 between average model predictions and data (Supplementary Table 3) are those with the largest model-predicted variability, due to the higher impact of stochastic effects in the capture process when mosquito abundance is low.

Supplementary Methods 5. Epidemiological Risk

After calibration of the larval carrying capacities, we run a stochastic implementation of the same model adding the transmission dynamics of arboviruses transmitted by the mosquito in the human hosts using a standard SEI-SEIR approach. We used for each site 100 parameter values sampled from the posterior distributions of its carrying capacity estimated by the MCMC procedure and ran 100 stochastic iterations for each parameter. We used the parameter values also to compute the R0 value (equation 4, Supplementary Table 4). The model equation for the mosquito population dynamics is reported in Supplementary Methods 1 (equation 1), while the model equations for the transmission dynamics for both dengue and chikungunya are reported below:

$$\begin{cases} \dot{V_S} = \frac{1}{2} d_P P - (m_V + \lambda_V) V_s \\ \dot{V_E} = -m_V V_E + \lambda_V V_s - \omega_V V_E \\ \dot{V_I} = -m_V V_I + \omega_V V_E \\ \dot{H_S} = -\lambda_H H_s \\ \dot{H_E} = \lambda_H H_s - \omega_H H_E \\ \dot{H_{IA}} = \omega_H (1 - p_s) H_E - \gamma H_{IA} \\ \dot{H_{IS}} = \omega_H p_s H_E - \gamma H_{IS} \\ \dot{H_R} = \gamma (H_{IS} + H_{IA}) \\ \dot{H_D} = p_d H_{IS} \end{cases} \quad (2)$$

where V_S , V_E and V_I are the number of vectors in different infection states (susceptible, exposed, and infected respectively). We assumed that once a mosquito becomes infectious, *ie* it bites in the infectious host, it survives "the extrinsic incubation period", it remains infectious until its death, without vertical transmission to eggs. H_S, H_E, and H_R represent, respectively, the infection states for the human host, namely susceptible, exposed and recovered. The H_S was human population size associated with each site of entomological data collection, corresponding to a spatial polygon of 300m circular buffer, was derived from single census units

(http://dati.istat.it), using a focal filtering approach. Human inhabitants within a circular buffer of radius 150 m, drawn around each cell of size 10 x 10 m, falling within the site polygons, were calculated using a weighted spatial overlapping method from census units. For each site, the cell with the highest value was considered as the human population size. We assumed homogenous mixing and a constant human population. Humans may acquire infection at a rate λ_H, become infectious after an average time called "intrinsic incubation period" given by $1/\omega_H$, and become lifelong immune after recovery with a rate γ. Therefore, the force of infection on humans λ_H is:

$$\lambda_H = \beta\varphi\ \chi_H \frac{V_I}{N} \quad (3)$$

where β is the mosquito biting rate, φ is the host preference and χ_H is the probability that a human becomes infected upon a single bite from an infectious mosquito. The classes H_{IA}, and H_{IS} is asymptomatic and symptomatic cases, respectively. The H_E become symptomatic case with probability p_s. Finally, H_D represent the fraction of H_{IS} detected by the surveillance system with notification probability p_d. We considered temperature-dependent extrinsic incubation periods and per-bite transmission probabilities for dengue, whereas only temperature-independent estimates were available for chikungunya (Supplementary Table 5). The transmission model was initialized, for each stochastic run, with a single infectious human, representing an imported case at a date sampled uniformly between May and November. All parameter values were sampled from the prior distribution listed in Supplementary Table 5.

The simulated *Ae. albopictus* females population and the sampled parameters were used to compute the basic reproduction number R_0, which represents the number of human secondary cases caused by a primary human infector, according to the equation:

$$R_0 = (\beta\phi)^2 \frac{V}{N_H} \frac{\chi_V \chi_H}{\gamma \mu_V} \frac{\omega_V}{\omega_V + \mu_V} \quad (4)$$

R_0 represents the expected number of secondary cases infected by an index case in a fully susceptible population. When $R_0 > 1$, the epidemic may spread, with intensity proportional to its value. This interpretation assumes that the reduction in susceptible individuals is negligible in the early epidemic phase, leading to exponential growth. While R_0 can be approximated using models of transmission dynamics between the mosquito vector and human host, such estimates should be carefully interpreted in sparsely populated areas.
As such, we computed R_0 values only for sites with a human population density of at least 30 residents per hectare. According to this approach we excluded from the analysis the following two sites:

- Muratella which is a commercial site inside the Metropolitan area of Rome, characterized by a high density of office buildings and enterprises, making it a significant business hub where people are transitional and move in and out during the day,
- Roma Aurelia which is a peripheric residential neighbourhood encompassed by wide green spaces that are also frequented by visitors from outside the neighbourhood.

Supplementary Table 1

Description	Parameter	Value/Formula	Reference
Mortality rate	m_E	$506\text{-}506*e^{-(\frac{T-25}{27.3})\wedge 6}$	[7]
	m_L	$0.029\text{-}858*e^{-(T-43.4)}$	
	m_P	$0.021\text{-}37*e^{-(T-36.8)}$	
	m_V	$0.031\text{-}95820*e^{-(T-50.4)}$	
Length gonotrophic cycle	d_E	$\frac{1}{6{,}9 - 4 * e^{-(\frac{T-20}{4{,}1})\wedge 2}}$	[7]
	d_L	$\frac{1}{0{,}12T^2 - 6{,}6T + 98}$	
	d_P	$\frac{1}{0{,}027T^2 - 1{,}27T + 27{,}7}$	
	d_V	$\frac{1}{0{,}046T^2 - 2{,}77T + 45{,}3}$	
Capture rate	b	1.1164*10^(-4)	[6]
Correction factor for adult mortality	σ	2.06 (95% CI 1.97-2.14)	[3]
N eggs	n_E	60	[3]

Supplementary Table 1: Biological parameters. T denotes the temperature in Celsius degree.

Supplementary Table 2

Site	**Larval carrying capacity**			
	2012		2023	
	Mean	95% CI	Mean	95% CI
Muratella	141.31	122.68-162.69	214.46	197.78-232.66
Villa Bonelli	152.76	134.4-172.02	232.05	213.01-252
Trastevere	103.74	92.43-116.86	391.2	364.67-419.97
Cornelia	175.15	158.42-192.93	197.36	178.92-217.44
Cipro	187.82	169.05-207.19	383.07	359.11-408.75
Flaminio	46.48	38.46-55.19	121.75	106.94-137.61
Vittorio Emanuele	347.12	325.6-370.53	495.85	466.27-525.74
Arco di Travertino	180.1	165.49-196.43	326.64	304.91-350.69
Nomentano	520.27	490.53-550.08	365.42	341.41-391.17
Nuovo Salario	192.31	175.51-212.19	417.39	391.86-443.93
Roma Aurelia	-	-	231.88	213.18-251.12
Roma S. Pietro	-	-	296.42	273.87-318.3
Subaugusta	-	-	758.87	711.69-805.69
Sapienza	-	-	230.43	213.59-250.29

Supplementary Table 2: Estimated site- and year-specific larval carrying capacity.

Supplementary Table 3

Sites	R^2	
	2012	**2023**
Muratella	0. 09350538	0. 5532686
Villa Bonelli	0.56758690	0.5750779
Trastevere	0.34339602	0.6268744
Cornelia	0.68559732	0.6369229
Cipro	0.50290772	0.8128448
Flaminio	0.39976155	-0.1019623
Vittorio Emanuele	0.51760103	0.5376999
Arco di Travertino	0.25523571	0.7254676
Nomentano	0.55816261	0.6533689
Nuovo Salario	0.35428973	0.5111843
Roma Aurelia	-	0.7429946
Roma S. Pietro	-	0.6384366
Subaugusta	-	0.5929463
Sapienza	-	0.2811612

Supplementary Table 3: Metric (R^2) for the goodness of fit between predicted and observed mosquito abundances.

Supplementary Table 4

Sites	R0 DENV (95% CI)		R0 CHIKV (95% CI)	
	2012	2023	2012	2023
Villa Bonelli	0.09(0.05-0.15)	0.26(0.14-0.42)	0.20(0.08-0.35)	0.33(0.14-0.57)
Trastevere	0.18(0.09-0.29)	0.70(0.37-1.11)	0.22(0.09-0.39)	0.75(0.33-1.29)
Cornelia	0.24(0.13-0.38)	0.31(0.16-0.49)	0.44(0.19-0.75)	0.38(0.16-0.66)
Cipro	0.19(0.10-0.30)	0.50(0.26.0.79)	0.34(0.15-0.59)	0.60(0.26-1.04)
Flaminio	0.50(0.26-0.81)	0.91(0.48-1.46)	0.61(0.262-1.07)	**1.1(0.47-1.88)**
Vittorio Emanuele	0.54(0.29-0.85)	0.73(0.39-1.16)	0.77(0.33-1.31)	0.79(0.35-1.35)
Arco di Travertino	0.35(0.18-0.55)	**1.1(0.59-1.75)**	0.50(0.21-0.85)	**1.2(0.52-2.03)**
Nomentano	0.62(0.33-0.98)	0.50(0.27-0.8)	**1.03(0.45-1.76)**	0.54(0.23-0.93)
Nuovo Salario	0.60(0.32-0.95)	**1.72(0.92-2.71)**	**1.14(0.50-1.96)**	**2.24(0.97-3.82)**
Roma S. Pietro	NA	0.77(0.41-1.22)	NA	0.93(0.40-1.59)
Subaugusta	NA	0.40(0.21-0.64)	NA	0.59(0.26-1.01)
Sapienza	NA	**1.03(0.55-1.62)**	NA	**1.11(0.48-1.9)**

Supplementary Table 4: Estimated R0 for DENV and CHIKV (median between June 1st and September 30th) for sites inside the GRA in 2012 and 2023. In bolt the sites in which R0 is above the epidemic threshold (R0>1).

Supplementary Table 5

Pathogens	Parameters	Description	Distribution	Min ;Max	Refs
CHIKV	β	Biting rate (bite/mosquito/day)	Uniform	0.08;0.10	[3]
	ϕ	Vector preference (%)	NA	0.6[$]	[9–11]
	-	Date of imported infection	Uniform	1 May; 15 November	-
	χ_H	Probability of vector-to-human transmission per bite (%)	Uniform	75;80	[12]
	χ_V	Probability of human-to-vector transmission per bite (%)	Uniform	50;55	[12]
	ω_V	Extrinsic incubation period (days^{-1})	Uniform	2;3	[13]
	ω_H	Intrinsic incubation period (days^{-1})	Uniform	1;12	[14]
	γ	Human infectious period (days)	Uniform	2;7	[14]
	p_s	Probability of developing symptoms (%)	Uniform	65;93	[15]
	p_d	Probability of being detected (%)	Uniform	44;80	[15]
	-	Delay between symptom onset and detection(days)	Gamma	shape=1.248; scale=18.963	[16]
	β	Biting rate (bite/mosquito/day)	Uniform	0.08;0.10	[3]
	ϕ	Vector preference (%)	NA	mean=0.6	[9–11]
	-	Date of imported infection	Uniform	1 May; 15 November	-
DENV	χ_H	Probability of vector-to-human transmission per bite (%)	NA	7.35*10^(-4) *T*(T-15.84)*$\sqrt{36.40 - T}$	[17]
	χ_V	Probability of human-to-vector transmission per bite (%)	NA	4.39*10^ (-4) *T*(T-3.62)*$\sqrt{36.82 - T}$	[17]
	ω_V	Extrinsic incubation period (days^{-1})	NA	1.09*10^(-4) *T*(T-10.39)*$\sqrt{43.05 - T}$	[17]
	ω_H	Intrinsic incubation period (days^{-1})	Uniform	3;10	[18]
	γ	Human infectious period (days)	Uniform	2;5	[19]
	p_s	Probability of developing symptoms (%)	Uniform	25;70	[20]
	p_d	Probability of being detected (%)	Uniform	44;80	[15]
	-	Delay between symptom onset and detection(days)	Gamma	shape=1,248;scale=18,963	[16]

Supplementary Table 5: Epidemiological parameters for chikungunya and dengue. *T* denotes the temperature in degree Celsius. [$]= mean value obtained from reference.

Supplementary Figure 1

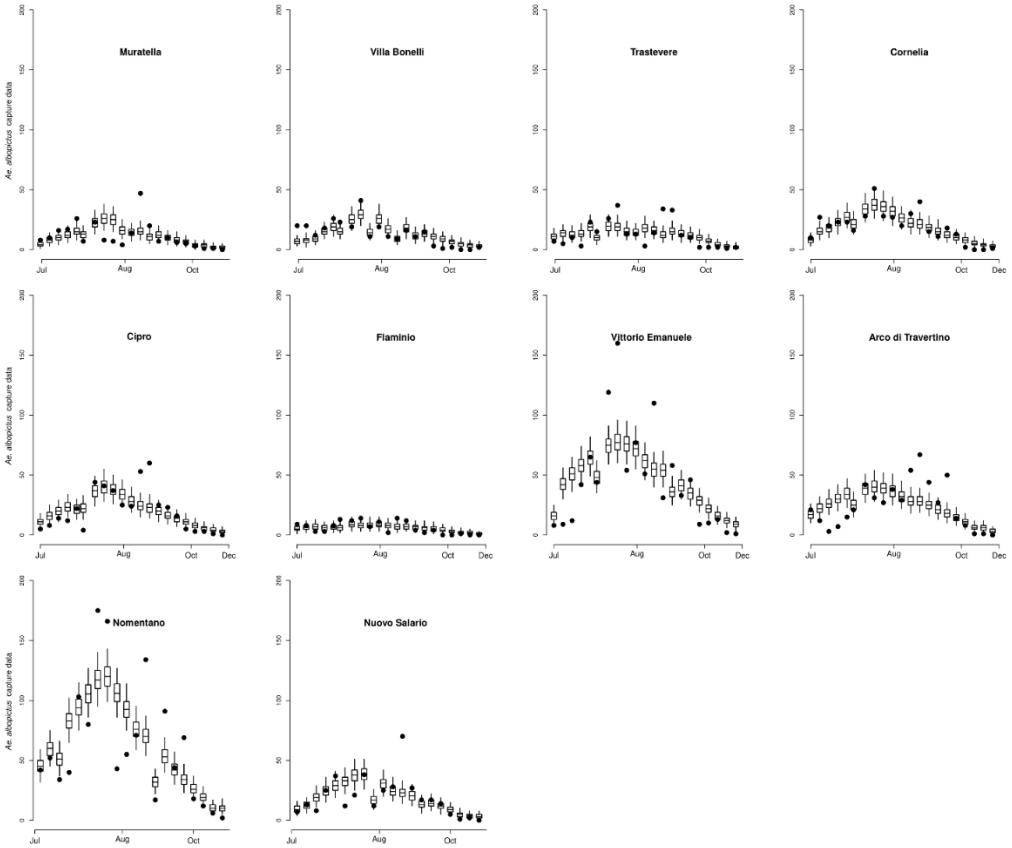

Supplementary Figure 1: comparison between observed (black point) and estimated (boxplots; median and Interquartile) total number of capture *Ae. albopictus* female each week for the 10 study sites in 2012 calculated over 60 samples of the posterior distribution of free parameter (carrying capacity) and 20 stochastic iterations.

Supplementary Figure 2

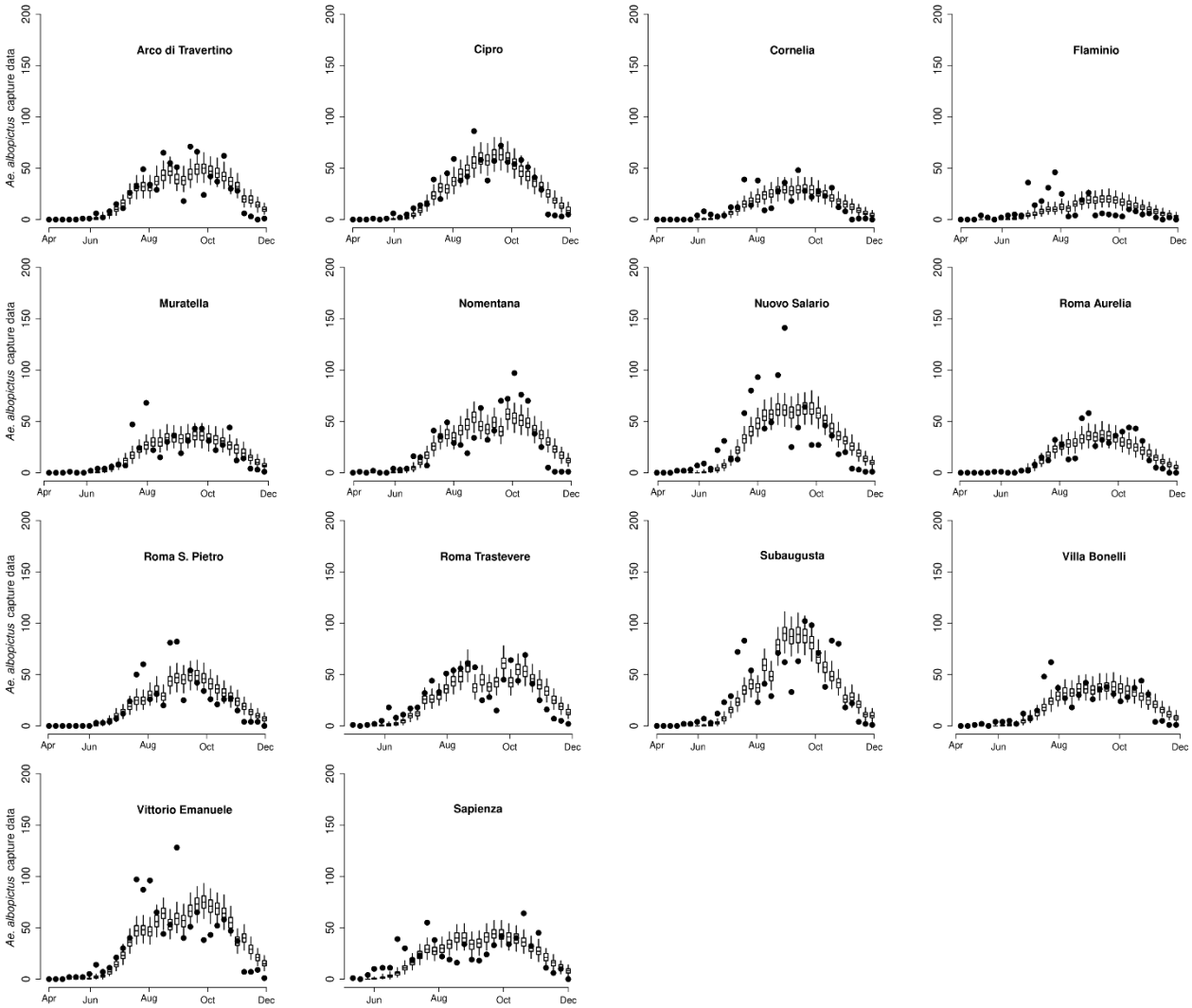

Supplementary Figure 2: comparison between observed (black point) and estimated (boxplots; median and Interquartile) total number of capture *Ae. albopictus* female each week for the 14 study sites in 2023 calculated over 60 samples of the posterior distribution of free parameter (carrying capacity) and 20 stochastic iterations.

Supplementary Figure 3

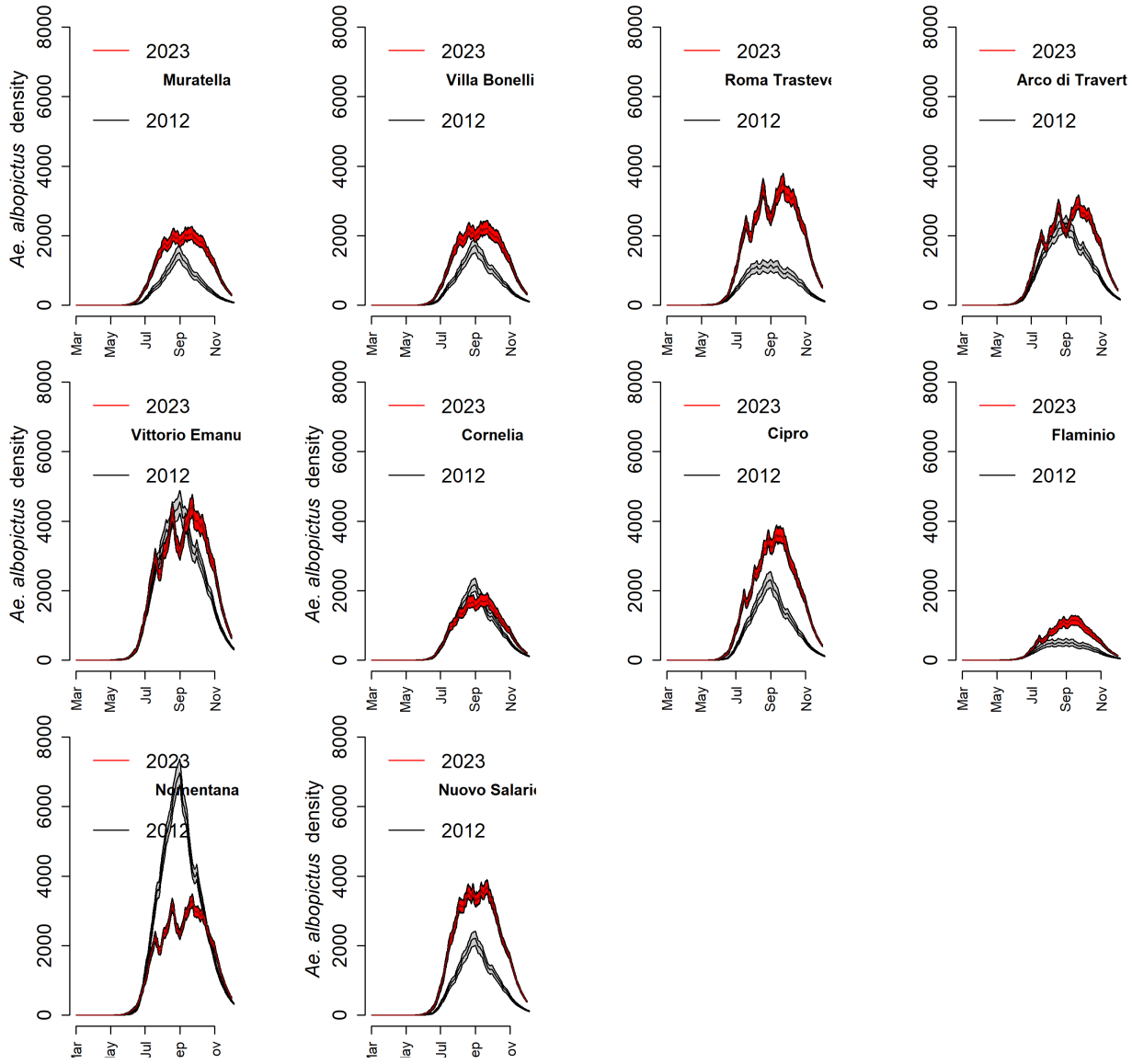

Supplementary Figure 3: Daily posterior distribution of adult *Ae. albopictus* females/hectare in each site sampled both in 2012 (grey) and 2023 (red).

Supplementary Figure 4

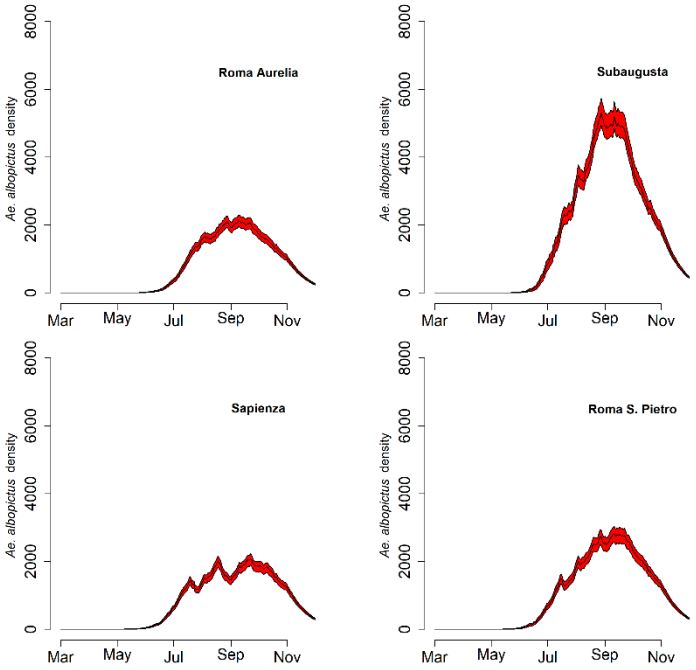

Supplementary Figure 4: Daily posterior distribution of adult *Ae. albopictus* females/hectare in newly sampled site in 2023.

Supplementary Figure 5

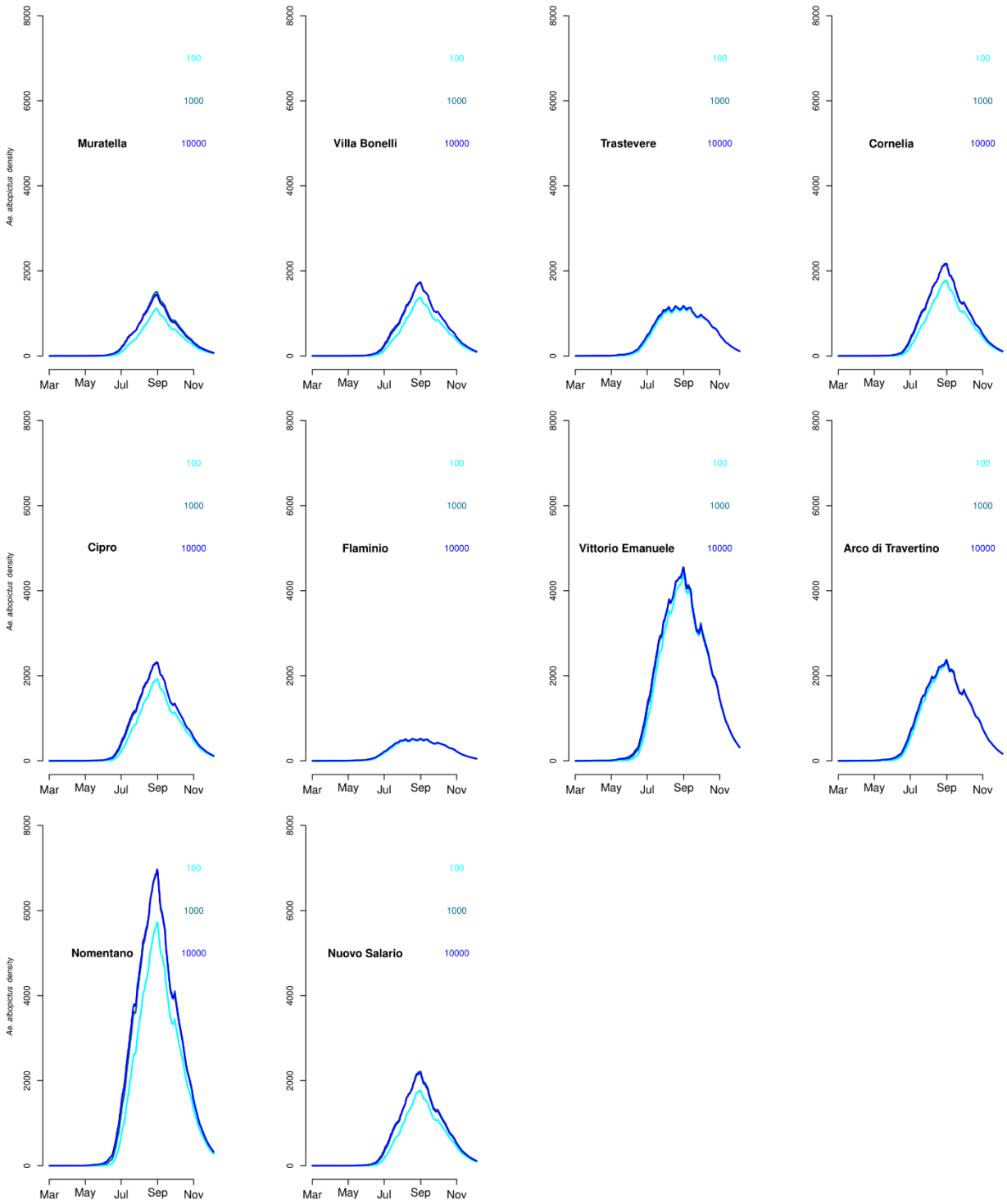

Supplementary Figure 5: Sensitivity analysis for 2012 entomological data. x-axis=months, y-axis=estimated *Ae. albopictus* females/hectare

Supplementary Figure 6

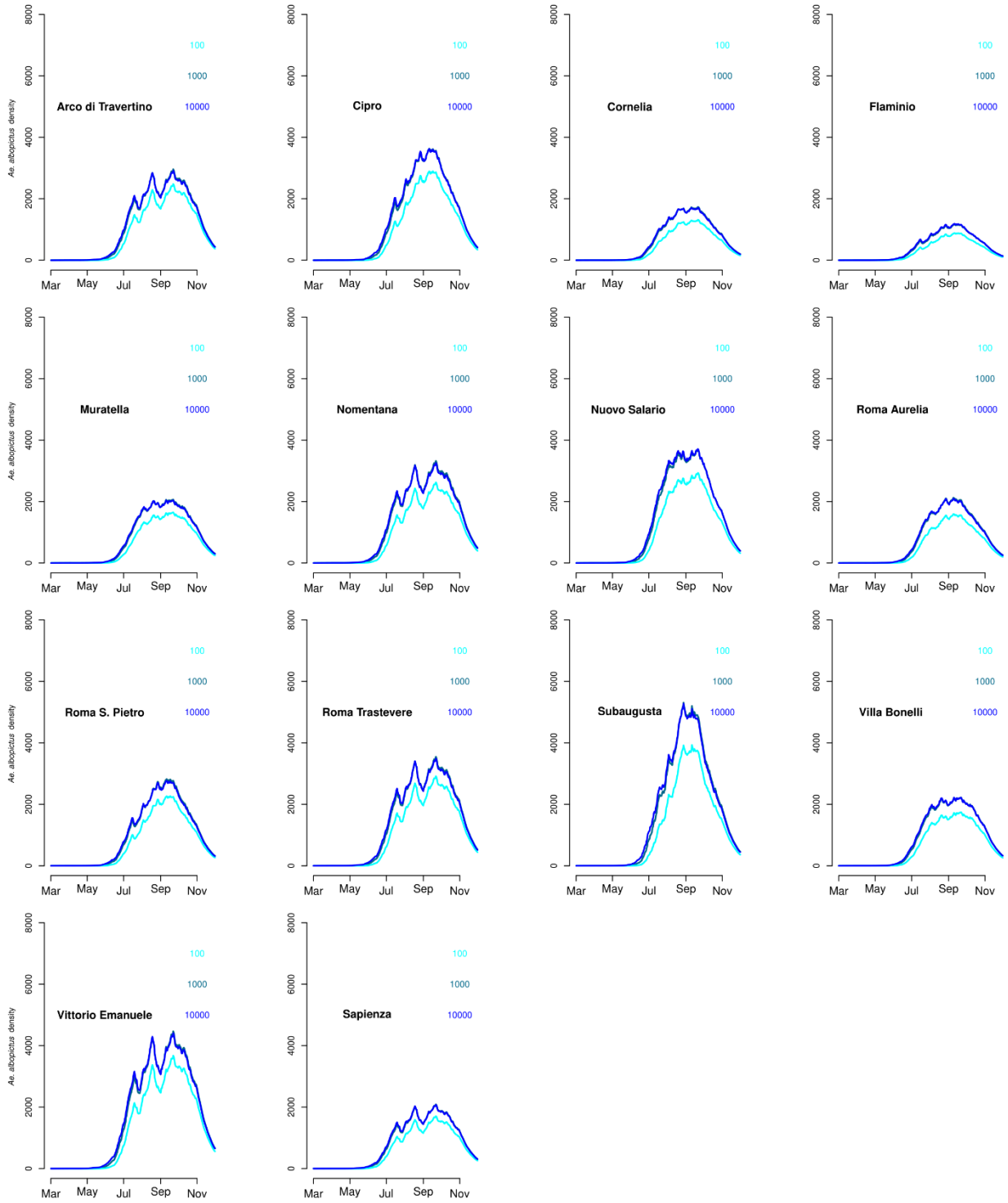

Supplementary Figure 6: Sensitivity analysis for 2023 entomological data. x-axis=months, y-axis=estimated *Ae. albopictus* females/hectare

Supplementary Figure 7

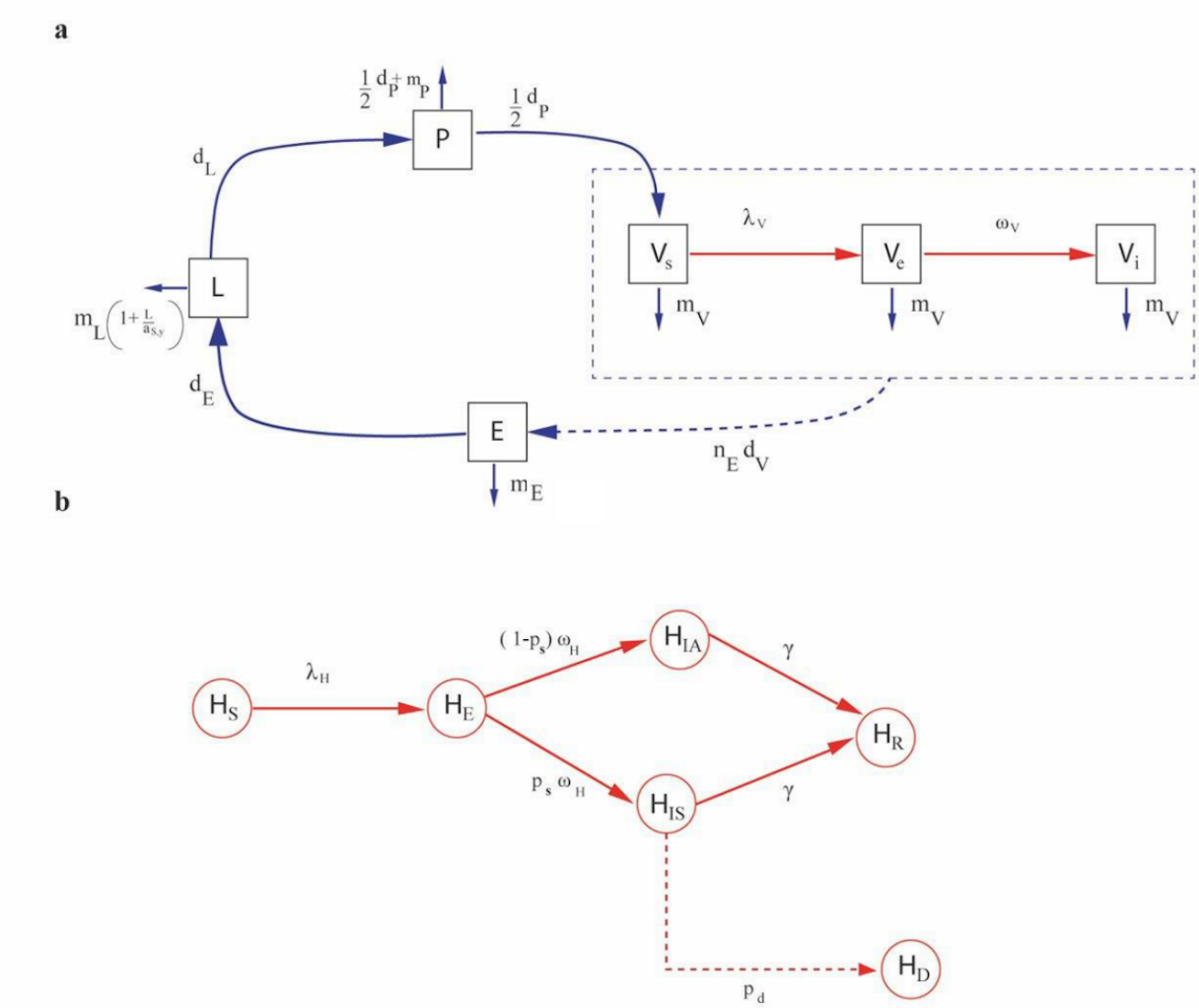

Supplementary Figure 7: **a** Model describing the evolution of the four life stages of the mosquito vector (description of variable was available in Supplementary Methods 1 and Supplementary Table 1), coupled to the epidemic transmission model in vectors (description of variable was available in Supplementary Methods 5 and Supplementary Table 5). The dashed blue box and arrow refer to oviposition. **b** Model describing the epidemic transmission in humans (description of variable was available in Supplementary Methods 5 and Supplementary Table 5).

Supplementary Figure 8

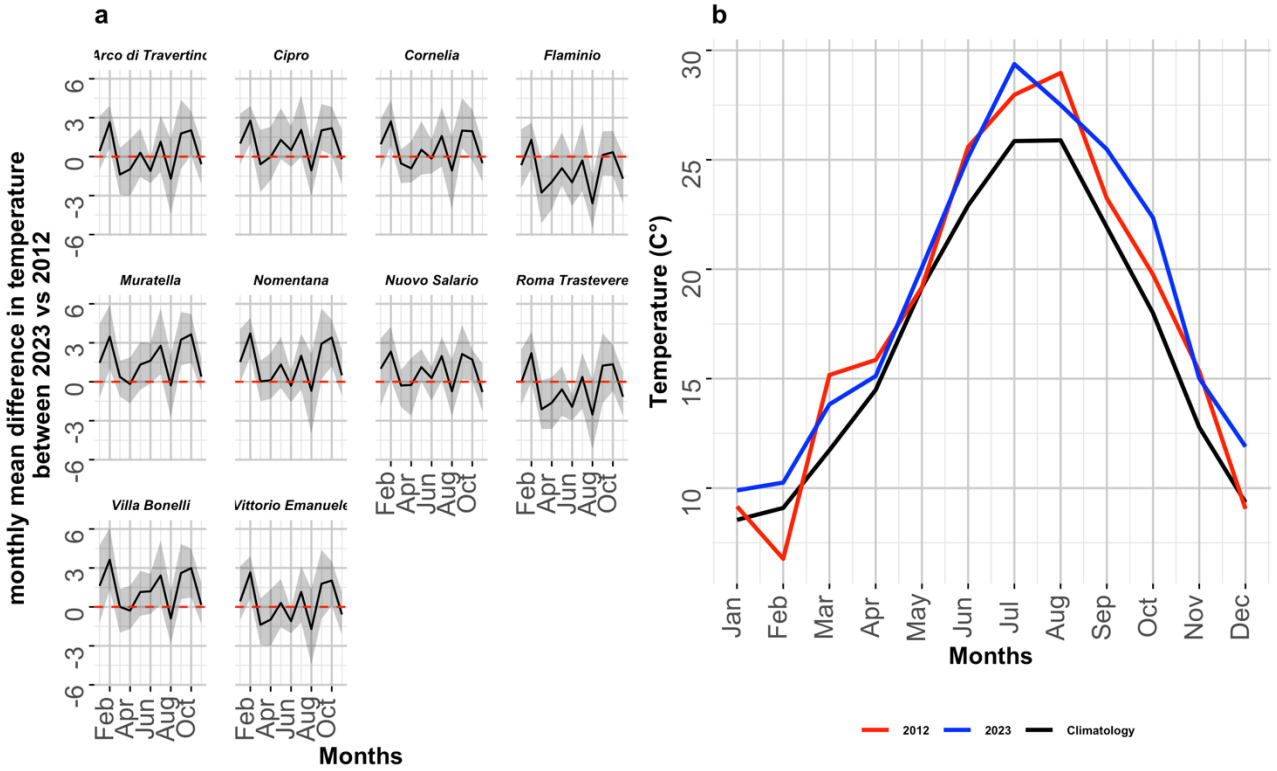

Supplementary Figure 8: a x-axis = Months, y-axis = Monthly average difference in temperature for each 10 common study sites between the two years. solid line is the mean; dashed area is the quantile. **b** Monthly average air temperature, calculated from meteorological data acquired at Roma Macao weather station near Sapienza site, for year 2012, 2023 and climatology normal for the period 1981-2010.

Supplementary References

1. Morabito, M. et al. The impact of built-up surfaces on land surface temperatures in Italian urban areas. *Sci. Total Environ.* **551–552**, 317–326 (2016).
2. Battista, G., Evangelisti, L., Guattari, C., Roncone, M. & Balaras, C. A. Space-time estimation of the urban heat island in Rome (Italy): Overall assessment and effects on the energy performance of buildings. *Build Environ* **228**, 109878 (2023).
3. Manica, M. et al. Transmission dynamics of the ongoing chikungunya outbreak in Central Italy: From coastal areas to the metropolitan city of Rome, summer 2017. *Euro Surveill.* **22**, 17-00685 (2017).
4. Guzzetta, G. et al. Potential Risk of Dengue and Chikungunya Outbreaks in Northern Italy Based on a Population Model of *Aedes albopictus* (Diptera: Culicidae). *PLoS Negl. Trop. Dis.* **10**, e0004762 (2016).
5. Facchinelli, L. et al. Development of a novel sticky trap for container-breeding mosquitoes and evaluation of its sampling properties to monitor urban populations of *Aedes albopictus*. *Med. Vet. Entomol.* **21**, 183–195 (2007).

6. Marini, F., Caputo, B., Pombi, M., Tarsitani, G. & Della Torre, A. Study of *Aedes albopictus* dispersal in Rome, Italy, using sticky traps in mark-release-recapture experiments. *Med. Vet. Entomol.* **24**, 361–368 (2010).
7. Poletti, P. et al. Transmission Potential of Chikungunya Virus and Control Measures: The Case of Italy. *PLoS One* **6**, e18860 (2011).
8. Delatte, H., Gimonneau, G., Triboire, A. & Fontenille, D. Influence of Temperature on Immature Development, Survival, Longevity, Fecundity, and Gonotrophic Cycles of *Aedes albopictus*, Vector of Chikungunya and Dengue in the Indian Ocean. *J. Med. Entomo.l* **46**, 33–41 (2009).
9. Caminade, C. et al. Global risk model for vector-borne transmission of Zika virus reveals the role of El Niño 2015. *Proc. Natl. Acad. Sci. U S A* **114**, 119–124 (2017).
10. Faraji, A. et al. Comparative Host Feeding Patterns of the Asian Tiger Mosquito, *Aedes albopictus*, in Urban and Suburban Northeastern USA and Implications for Disease Transmission. *PLoS Negl. Trop. Dis.* **8**, e3037 (2014).
11. Sivan, A., Shriram, A. N., Sunish, I. P. & Vidhya, P. T. Host-feeding pattern of *Aedes aegypti* and *Aedes albopictus* (Diptera: Culicidae) in heterogeneous landscapes of South Andaman, Andaman and Nicobar Islands, India. *Parasitol. Res.* **114**, 3539–3546 (2015).
12. Fortuna, C. et al. Vector competence of *Aedes albopictus* for the Indian Ocean Lineage (IOL) chikungunya viruses of the 2007 and 2017 outbreaks in italy: A comparison between strains with and without the E1:A226V mutation. *Euro Surveill,* **23**, 1800246 (2018).
13. Dubrulle, M., Mousson, L., Moutailier, S., Vazeille, M. & Failloux, A. B. Chikungunya Virus and Aedes Mosquitoes: Saliva Is Infectious as soon as Two Days after Oral Infection. *PLoS One* **4**, e5895 (2009).
14. Thiberville, S. D. et al. Chikungunya fever: Epidemiology, clinical syndrome, pathogenesis and therapy. *Antiviral Res*. **99**, 345–370 (2013).
15. Moro, M. L. et al. Chikungunya Virus in North-Eastern Italy: A Seroprevalence Survey. *Am. J. Trop. Med. Hyg.* **82**, 508 (2010).
16. Manica, M. et al. Reporting delays of chikungunya cases during the 2017 outbreak in Lazio region, Italy. *PLoS Negl. Trop. Dis.* **17**, e0011610 (2023).
17. Mordecai, E. A. et al. Detecting the impact of temperature on transmission of Zika, dengue, and chikungunya using mechanistic models. *PLoS Negl. Trop. Dis.* **11**, e0005568 (2017).
18. Chan, M. & Johansson, M. A. The Incubation Periods of Dengue Viruses. *PLoS One* **7**, e50972 (2012).
19. Marini, G. et al. Effectiveness of Ultra-Low Volume insecticide spraying to prevent dengue in a non-endemic metropolitan area of Brazil. *PLoS Comput. Biol.* **15**, e1006831 (2019).
20. Ferguson, N. M. et al. Benefits and risks of the sanofi-pasteur dengue vaccine: Modeling optimal deployment. *Science* **353**, 1033–1036 (2016).